DR · 323

UCRL-52778 Part 2

DEVICES FOR LAUNCHING 0.1-g PROJECTILES TO 150 km/s OR MORE TO INITIATE FUSION

Part 2, Railgun Accelerators

R. S. Hawke

July 6, 1979

Work performed under the auspices of the U.S. Department of Energy by the UCLLL under contract number W-7405-ENG-48.

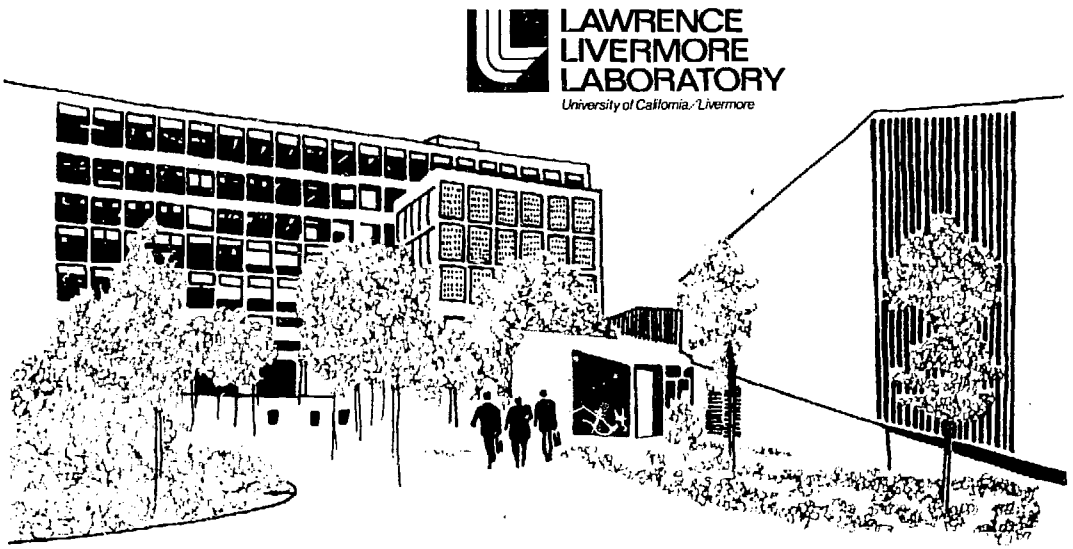

Distribution Category
UC-21

LAWRENCE LIVERMORE LABORATORY
University of California/Livermore, California/94550

UCRL-52778 Part 2

DEVICES FOR LAUNCHING 0.1-g PROJECTILES TO 150 km/s OR MORE TO INITIATE FUSION

Part 2, Railgun Accelerators

R. S. Hawke

Manuscript date: July 6, 1979

FOREWORD

Part 1 of this report summarizes J. N. Brittingham's feasibility investigation of using magnetic-gradient and electrostatic accelerators to launch 0.1-g projectiles to hypervelocities (150 km/s or more). This second part summarizes a similar investigation of the electromagnetic railgun. It then summarizes and compares the three types of accelerators. Because of the critical effect of boundary-layer drag on railgun performance, A. C. Buckingham did a separate study (summarized as Appendix A). Appendix B briefly comments on the suitability of three more methods of accelerating projectiles to hypervelocity.

CONTENTS

DEVICES FOR LAUNCHING 0.1-g PROJECTILES TO 150 km/s OR MORE TO INITIATE FUSION

Part 2, Railgun Accelerators

ABSTRACT

I explored the possibility of using a railgun accelerator to launch 0.1-g projectiles to hypervelocities (150 km/s or more) to initiate thermonuclear fusion. My analysis revealed that a railgun with a plasma-arc armature is a viable approach to the goal. When calculating the railgun's probable performance, I discovered that this launch system might possibly be designed to avoid adverse effects from boundary layer drag. An appendix provided by A. C. Buckingham summarizes his calculations that predict the amount of erosive drag between projectile and rail. Finally, I found that certain properties of railgun and projectile materials can impose operational limits. Using these limits, I designed single- and multistage accelerators. Within such limits, a railgun could accelerate a 0.1-g projectile to hypervelocities.

1. INTRODUCTION

The promise of abundant energy has inspired many approaches to controlled thermonuclear fusion. Pellets, ignited one per second, could be the energy source for power plants producing billions of watts of electrical power. To achieve ignition, one would have to deliver about 1 MJ of energy to a deuterium-tritium (DT) pellet in about 10 ns. Candidate igniters have included laser, electron, and heavy- and light-ion beams.

Another approach would be to ignite the pellet with the impact of projectiles weighing about 0.1 g. These projectiles could be accelerated to hypervelocity (150 km/s or more) by magnetic accelerators.[1-10] The advantage of a projectile is that the energy would be concentrated into a small volume. If the projectile moves rapidly enough to contain the energy, then it would be easy to deliver the energy in the required 10 ns by making the projectile short.

To bring us closer to the above goal, I have explored the electromagnetic railgun as a possible launch device.[11] My study represents Part 2 of a larger investigation into launch devices. In my part of the report, I describe the critical factors seen as limits on railgun accelerator design and operation.

With these limits in mind, I calculate the railgun's probable performance. Section 2 of my report presents my analysis of such an accelerator, Section 3 summarizes the results, and Section 4 briefly compares three of the accelerators considered in the combined investigation.

From my work, I conclude that the railgun offers a viable way to accelerate projectiles to 150 km/s or more. Thus, I think it deserves experimental pursuit.

2. RAILGUN ACCELERATOR

A railgun accelerator is a linear dc motor consisting of a pair of rigid, field-producing conducting rails and a movable conducting armature. The armature is accelerated as a result of the Lorentz force produced by the current, I, in the armature interacting with the magnetic field, B, of the rail currents (Fig. 1).

In 1964, researchers at MB Associates used a 28-kJ capacitor bank as a primary energy-storage device (PESD) and accelerated 5- and 31-mg nylon cubes to about 5 to 6 km/s with a plasma arc.[12] They also used an explosively

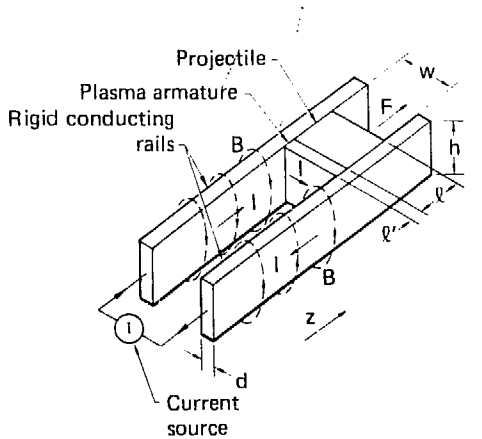

FIG. 1. Railgun accelerator.

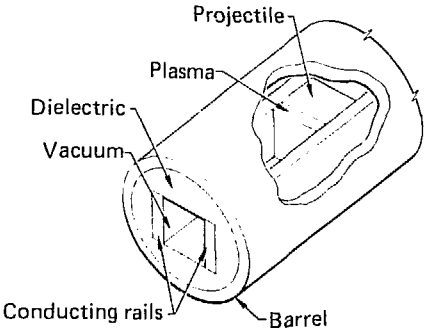

FIG. 2. Railgun assembly. The dielectric maintains the rail position and, along with the rails, confines the plasma behind the projectile.

imploded magnetic-flux compressor as a PESD and accelerated a copper sabot* and a steel projectile, with a total mass of 0.21 g, to a velocity of 9.5 km/s.[13]

Recently, researchers at the Australian National University at Canberra used a homopolar generator to store 900 kJ of energy in an inductor. The energy in the inductor was then used to accelerate a 3-g, 1/2-in. cube of Lexan dielectric to 5.9 km/s, again using a plasma arc.[14]

In the analysis that follows, the armature modeled is a thin plasma arc that impinges on the backside of a dielectric projectile and accelerates it. The arc is presumed to be confined behind the projectile by conducting rails on two sides and dielectric rail spacers between (Fig. 2).

2.1 ACCELERATOR DESIGN

2.1.1 Principles of Operation

Components. The components of a typical railgun system are shown in Fig. 3. A PESD, such as a capacitor bank or homopolar generator, is used to generate a current in the storage inductor, L_0, after switch S1 is closed. When the desired, usually maximum, current is established in L_0, S2 is closed to isolate the PESD from the circuit. At this time, shuttle switch S3 (a sliding multifingered conductor between two busbars) is moved across the breach end of

*A carrier in which a payload is mounted to permit its launching.

the railgun. The fuse first allows current to flow without arcing as the shuttle traverses the breach.

The fuse vaporizes and establishes the initial plasma arc. The arc and projectile accelerate along the rails. Prior to the arc exiting the muzzle of the gun, crowbar switch S4 is closed to extinguish the plasma arc and avoid spurious arcing.

Accelerating projectiles with a plasma arc has several advantages over a sliding metallic conductor. First, the plasma easily maintains contact with the rails. Second, a conducting metallic armature resistively heats and melts. Third, sliding metal contacts experience large erosive drag forces (Appendix A). Hence, the modeling discussed below is for a plasma arc armature.

Simulation Code. The railgun simulation code[15] combines (1) equations of motion, (2) circuit equations, and (3) energy distribution.

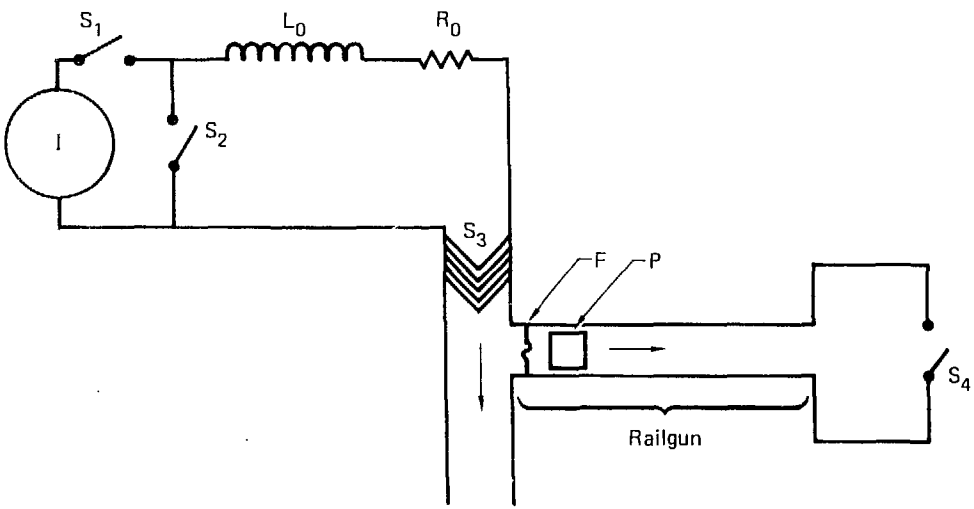

FIG. 3. Components of a railgun system: I, current source (HPG or capacitor bank); L_0, storage inductor; R_0, circuit resistance; F, fuse; P, projectile; S_1, coil-charging switch; S_2, source crowbar; S_3, shuttle switch; and S_4, armature crowbar. (Note: S_3 is not needed when a capacitor bank is used as a current source.)

Equations of Motion. Acceleration, a, is given by

$$a = \int_0^w \frac{\bar{I} \cdot d\bar{w} \times \bar{B}}{m} = \frac{L_l I^2}{2m} . \quad (1)$$

where I is the current in the arc, w is the rail spacing (Fig. 1), B is the magnetic-field intensity in the region of the arc, m is the mass of the projectile, and L_l is the inductance per unit length of the railgun.

The projectile velocity, v, is given by

$$v = \int a dt , \quad (2)$$

where t is time, and the projectile position, z, is given by

$$z = \int v dt . \quad (3)$$

Circuit Equations. At high current density, the plasma-arc voltage, V_A, is nearly independent of the arc current and equal to about 200 V.[16,17]

The voltage, V_I, resulting from the time variations of the current and inductance, L, of the railgun, is given by

$$V_I = \frac{d(LI)}{dt} = L\frac{dI}{dt} + I\frac{dL}{dt} . \quad (4)$$

And since

$$L = L_l z , \quad (5)$$

then

$$\frac{dL}{dt} = L_l v . \quad (6)$$

The voltage, V_R, along the two rails is given by

$$V_R = 2 \int_0^z IRdz , \quad (7)$$

where R is the resistance of each rail. More[18] used iterative calculations to determine the temperature, resistivity, current diffusion, and resistance of the rails as functions of current density and time. These are described below.

Figure 4 shows the equivalent circuit of the railgun during projectile acceleration. Using Kirchhoff's law, one obtains the relation

$$IR_0 + L_0\frac{dI}{dt} + IR + I\frac{dL}{dt} + L\frac{dI}{dt} + V_A = 0 \ , \tag{8}$$

from which the current and voltages are calculated. (Stray circuit resistance and inductance are included in R_0 and L_0, respectively.)

Distribution of Energy. The following equations are used to calculate the distribution of energy throughout the projectile's acceleration. The instantaneous energy, E_C, in the storage coil is

$$E_C = \frac{L_0 I^2}{2} \ . \tag{9}$$

The inductive energy, E_I, between the rails is given by

$$E_I = \frac{zL_1 I^2}{2} \ . \tag{10}$$

The energy loss, E_A, in the plasma arc is given by

$$E_A = \int V_A I dt \ . \tag{11}$$

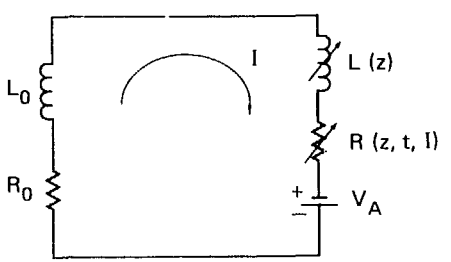

FIG. 4. Equivalent circuit of railgun and storage coil during acceleration of projectile. [R(z,t,I) and L(z) are the time-dependent resistance and inductance of the railgun.]

The energy loss, E_R, in the fixed circuit elements and rails is given by

$$E_R = \int I^2 R_0 dt + 2 \int I^2 R dt \ . \tag{12}$$

The instantaneous kinetic energy, E_p, of the projectile is given by

$$E_p = \frac{mv^2}{2} \ . \tag{13}$$

Figure 5 indicates the sequence of calculations used in the model.

2.1.2 Design Considerations: Operational Limits

The design and operation of a railgun is restricted by practical limits. These limits result from the properties of the rail and projectile materials, interior ballistics of the projectile, sustainable voltage without spurious arcing, and available energy.

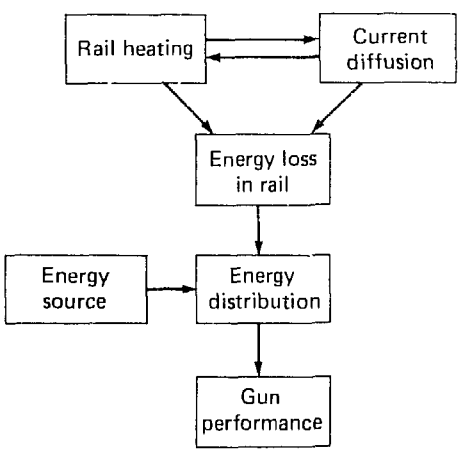

FIG. 5. Sequence of calculations used in simulation code.

Rail Melting. Melting of the rails is undesirable, and high temperatures decrease their strength. More[18] calculated the temperature rise and resistance of the rails as follows.

The current density, j, in the rails is given by

$$j = \frac{\partial H}{\partial x} , \tag{14}$$

where H is the magnetic field and x is the dimension normal to the rail surface. Because the dimensions of the rails are large compared with the current penetration depth, one-dimensional analysis is adequate.

The diffusion of H into the conductor is given by

$$\mu_0 \frac{\partial H}{\partial t} = \frac{\partial}{\partial x}\left(\eta \frac{\partial H}{\partial x}\right) \tag{15}$$

and

$$\rho C_v \frac{\partial T}{\partial t} = \frac{\partial}{\partial x}\left(k \frac{\partial T}{\partial x}\right) + \eta \left(\frac{\partial H}{\partial x}\right)^2 , \tag{16}$$

where μ_0 is the permeability, η is the resistivity, C_v is the specific heat, k is the thermal conductivity, and ρ is the mass density of the rails.

The electrical resistivity is assumed to be described by

$$\eta = \eta_0 + \alpha T , \tag{17}$$

where η_0 is the initial resistivity, α is the temperature coefficient, and T is the temperature.

Equations (14) through (17) are solved as implicit finite-difference equations,[19] producing the temperature profile and resistance of the rails as functions of time, rail dimensions, and current. The calculated rail resistance was used in the simulation code described above.

The maximum temperature rise occurs on the surface of the rails and is shown in Fig. 6 as a function of current per unit of rail perimeter $p = 2(h + d)$, where d is the rail thickness. Results are shown for two initial temperatures, T_0, and closely agree with Kidder's approximation[20]

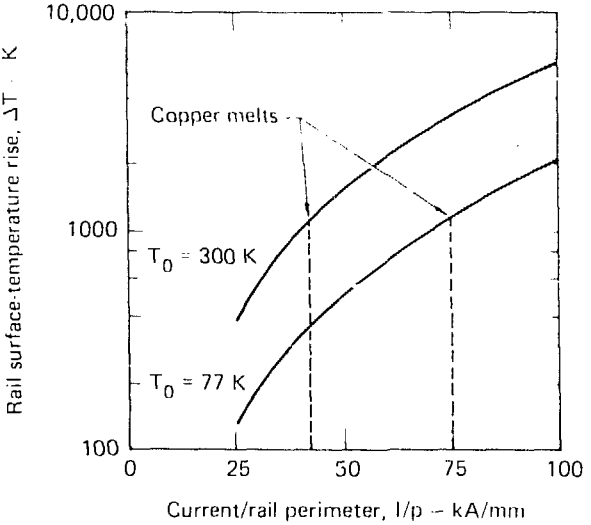

FIG. 6. Maximum temperature rise occurs on surface of rails.

$$\Delta T \sim \frac{2\mu_0 I^2}{\pi C_v p^2} \ln\left[1 + \frac{\pi}{2}\sqrt{\frac{C_v \eta_0}{\mu_0 k}}\right] . \qquad (18)$$

I conclude that for a copper rail system initially at room temperature, the perimeter current density may be limited to 43 kA/mm and that a rail system initially at liquid nitrogen temperature may be limited to 75 kA/mm.

Here I only considered the effects of a single launch. Rapid repetitive launching would require heat removal during railgun operation. This is discussed later.

Rail Deformation. Figure 7 shows the magnetic pressure on the rails as a function of the current per mm of rail spacing. To remain below the yield point of hardened steel, with an elastic strength of 0.7 GPa (10^5 psi), the current must remain less than 75 kA/mm of rail spacing. Copper plating on the steel would maintain electrical efficiency while the steel would provide the needed strength.

Careful design of the whole rail rail-support and barrel structure will be required to operate at the limit established by the elastic strength of the rail material.[15]

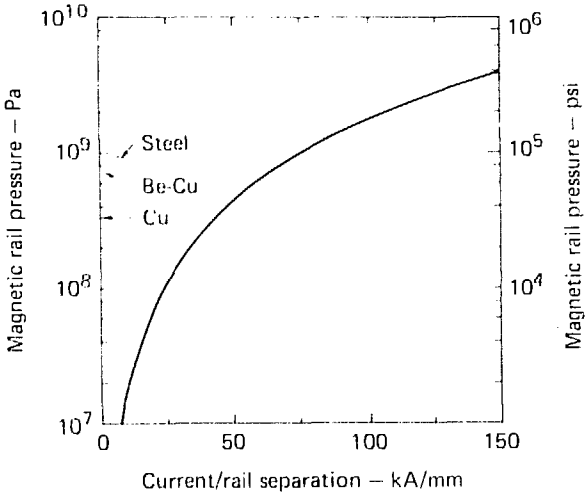

FIG. 7. Magnetic pressure on inside of rail surface increases with current per mm of rail spacing. Indicated are the elastic strengths of copper (Cu), beryllium-copper (Be-Cu), and steel.

Mechanical Integrity of the Projectile. The average pressure, P, on the backside of the projectile with surface area, A, is given by

$$P = \frac{ma}{A} = \frac{L_1 I^2}{2A} . \tag{19}$$

For a given elastic strength, σ_y, of a projectile, the maximum non-destructive acceleration, a_{max}, and current, I_{max}, are given by

$$a_{max} = \frac{\sigma_y A}{m} \tag{20}$$

and

$$I_{max} = \left[\frac{2\sigma_y A}{L_1} \right]^{1/2} . \tag{21}$$

To retain the mechanical integrity of a square-bore projectile with an elastic strength of 1.4 GPa (2×10^5 psi), the current must remain less than 81 kA/mm of rail spacing. The design of high strength, self-supporting projectiles has been demonstrated.[21] This is one of the key factors that will lead to successful railgun operation.

Because launcher performance improves with current (Eq. 1) and because current per unit spacing Fig. 7 and Eq. (21) and per unit perimeter (Fig. 6) have limits, it is desirable to maximize rail spacing and perimeter. The perimeter can be increased indefinitely on the outside portion of the rails, but the rail spacing governs the bore size (assumed to be square). It has been ex- perimentally found[22] that the aspect ratio, A_R, defined as the ratio of the length to the width and height of the projectile, must remain greater than 0.5 to maintain dynamic stability. Hence, increasing the bore results in a longer, larger, and more massive projectile, which in turn requires more input energy and a longer accelerator. Thus the choice of bore size is a compromise between competing factors that vary with the specific application.

Voltage Gradient Between the Rails. An arc discharge in front of or behind the arc driving the projectile would divert some or all of the remaining energy. This discharge must be avoided.

Available Energy. In addition to the above considerations, the performance of a railgun launcher is limited by the amount of energy available to it. Maximum available energy equals energy stored in the PESD less the energy loss incurred in transfers from the PESD tc che storage inductor and then to the railgun. The efficiency of converting electrical to kinetic energy with a railgun depends on several factors. This is discussed below for specific designs.

2.2 ACCELERATOR CALCULATIONS

2.2.1 Single-Stage Railgun

Bore Size. The above discussion pointed out that a higher current leads to a shorter accelerator and lower energy loss. The limit on current per unit rail spacing (75 kA/mm) requires a larger bore for higher currents. The limit on

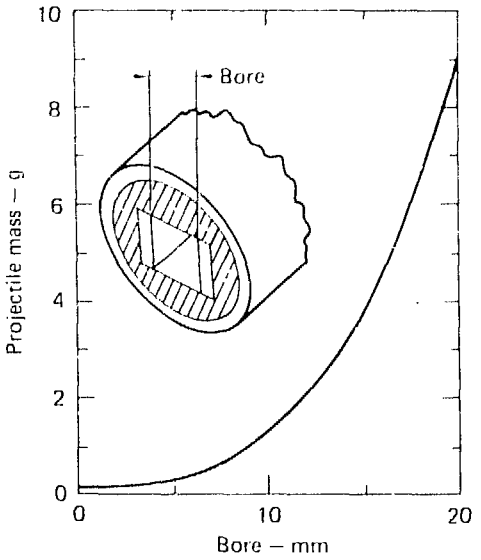

FIG. 8. Combined sabot and payload mass of projectile increases with bore size. (Sabot material density = 2.26 g/cm^3, aspect ratio = 0.5.)

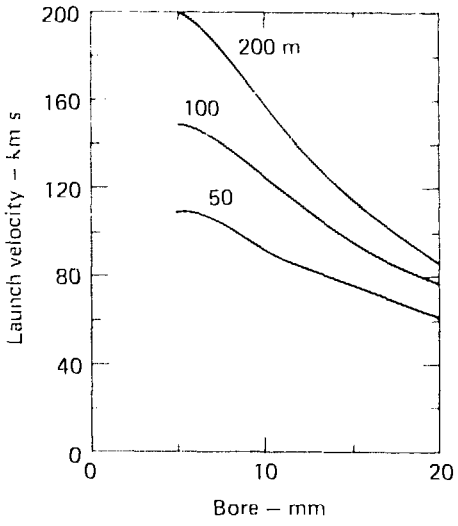

FIG. 9. Launch velocity of combined mass of sabot and payload for 50-, 100-, and 200-m-long accelerators. E_{C0} = 100 MJ; I_0/w = 75 kA/mm.

aspect ratio (0.5) requires a larger mass sabot for a larger bore. The larger mass requires more energy. Figure 8 shows the combined mass of the sabot and payload* vs bore size. The sabot material is assumed to have a density of 2.26 g/cm^3.

Figure 9 shows the launch velocity of the combined mass of the sabot with a 0.1-g payload vs bore size. The curves correspond to 50-, 100- and 200-m long accelerators. The initial current was 75 kA/mm of gun bore. The initial energy in the storage inductor was 100 MJ. Even though a larger bore permits higher current and hence acceleration force, a small bore is superior because of the smaller sabot mass required and resulting higher velocity.

A limit on how small the bore can be results from spurious arc breakdown. Figure 10 plots the maximum calculated values of the inductive, V_I, resistive, V_R, and total, V_T, voltages developed in the railgun as a

*The payload is the portion of the projectile that is useful for initiating fusion.

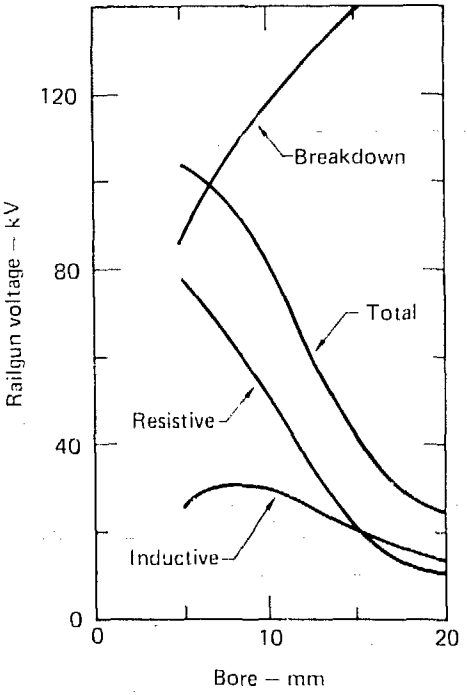

FIG. 10. Calculated maximum values of voltages developed in railgun. The maximum breakdown voltage is at pressures equal to or less than 10^{-4} torr. E_{C0} = 100 MJ; I_0/w = 75 kA/mm; length = 200 m.

function of bore size. The parameters are the same as in Fig. 9. The inductive voltage appears across the rails immediately behind the arc. The resistive voltage occurs along the rails from the arc toward the breach of the accelerator where the total voltage appears. The breakdown voltage[23] establishes the smallest bore that could be used without spurious arcing; in this example it is 6.7 mm. In the calculations that follow, I used 10 mm to provide a safety margin.

Performance With 10-mm Bore. Table 1 summarizes the limiting factors and limits used in calculations that follow. Table 2 lists the geometrical and physical parameters common to all these calculations.

Figure 11 shows the calculated exit velocity vs the initial energy E_{C0} stored in the storage inductor for several gun lengths. To achieve 150 km/s, one needs a minimum initial energy of 52 MJ in the storage inductor. Furthermore, PESD energy must be greater by the amount lost in charging the storage inductor. Typically 85% efficiency could be expected[24]; hence the PESD energy required would be about 60 MJ.

TABLE 1. Limiting factors and limits used in calculations.

Limiting factor	Limit	Value used
Railing melting (copper)	1083°C ⟶ I/p = 43 kA/mm	16 kA/mm
Rail yielding (steel)	1 GPa ⟶ I/w = 75 kA/mm	75 kA/mm
Sabot failure (graphite composite)	1.4 GPa ⟶ I/w = 81 kA/mm	75 kA/mm
Projectile stability	A_R = 0.5	0.5
Voltage breakdown	120 kV @ w = 10 mm	80 kV

TABLE 2. Geometrical and physical parameters used for calculations.

Parameter	Value used
Rail bore width (w)	10 mm
Rail bore height (h)	10 mm
Rail perimeter (p)	40 mm
Sabot length (ℓ)	5 mm
Sabot mass	1.13 g
Payload mass (m_{pl})	0.1 g
Projectile mass (m_T)	1.23 g
Initial current (I_0)	750 kA
Circuit resistance (R_0)	10 L_0

Figure 12 shows the launch velocity vs accelerator length for various initial energies in the storage inductor. The maximum launch velocity, v_{max}, would result if there were enough stored energy to maintain a constant current of 750 kA throughout acceleration. Consequently, the v_{max} curve also indicates the minimum-length accelerator needed to achieve a given velocity without exceeding the limits in Table 1. A velocity of 150 km/s would require an accelerator length of at least 115 m. When the stored energy is not adequate to maintain constant current, say for E_{C0} = 100 MJ, an accelerator length of about 200 m would be required.

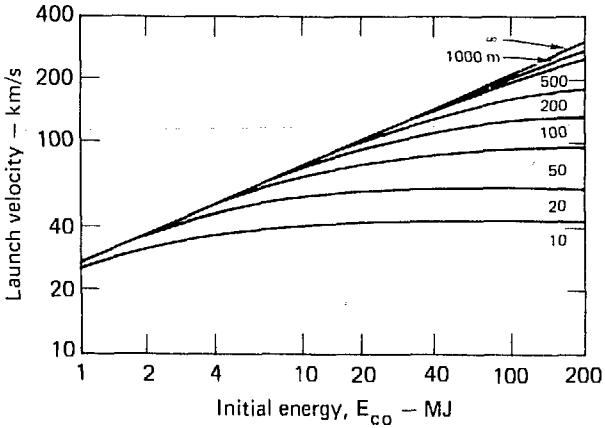

FIG. 11. A 150-km/s launch velocity needs a minimum initial energy of 52 MJ in the storage inductor. (Table 2 parameters.)

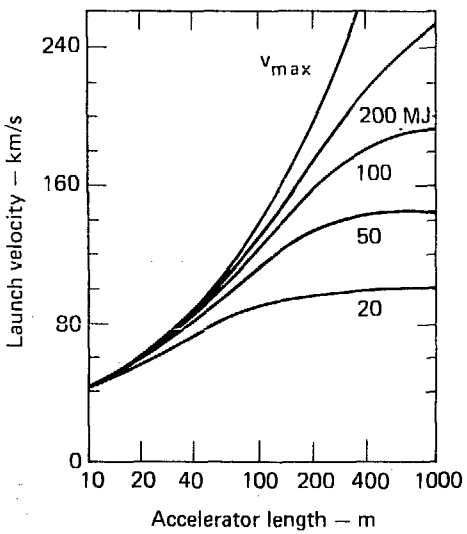

FIG. 12. A maximum launch velocity, v_{max}, would result if there were enough stored energy to maintain a constant current of 750 kA throughout acceleration. The curves below v_{max} indicate various initial energies stored in the inductor. (Table 2 parameters.)

Figure 13 plots the energy-transfer efficiencies of the combined projectile, ξ_p, and payload, ξ_{pl}, vs velocity, where

$$\xi_p = \frac{m_T v^2}{L_0 I_0^2} \tag{22}$$

and

$$\xi_{pl} = \frac{m_{pl} v^2}{L_0 I_0^2} . \tag{23}$$

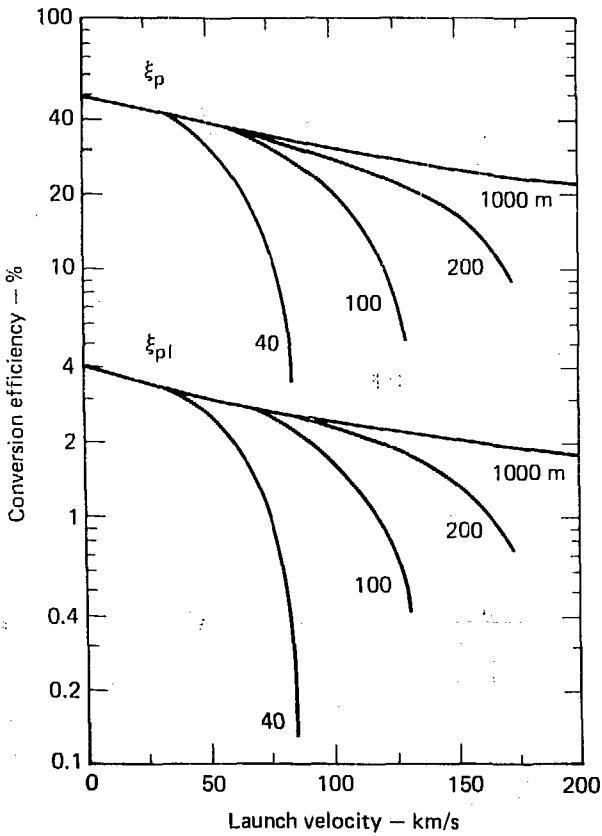

FIG. 13. Electrical-to-kinetic energy conversion efficiencies of combined projectile and payload for accelerators of various lengths. (Table 2 parameters.)

The efficiency of converting the initial energy stored in the inductor into kinetic energy of the payload can be 2% at 150 km/s. Note that if the kinetic energy of the sabot mass could be used as a payload, the efficiency would be about 25%.

2.2.2 Multistage Railgun (MSRG)

The earlier discussion has been limited to a single pair of rails, i.e., a single-stage railgun. In that case, approximately 50% of the energy stored in the inductor is lost in resistive heating of the rails. Dividing the accelerator into several, shorter, modular stages would

- Reduce the amount of energy loss in heating the rails.
- Allow the current to be reestablished at the highest usable value in each stage.
- Reduce the resistive voltage drop.
- Provide a convenient division of the total amount of required energy into smaller units.
- Lead to an accelerator that could be built by adding a few stages at a time.

The only disadvantage of an MSRG railgun is that it is more complex.

Energy Savings. Figure 14 shows the relative energy loss distributed in the rails behind the projectile when the projectile has traveled either half or

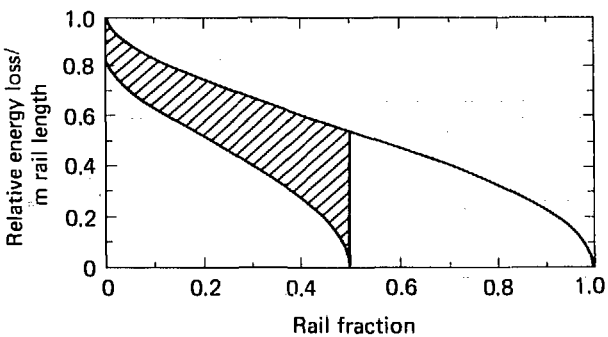

FIG. 14. Energy density loss in rails behind projectile that has traversed either half or all the accelerator length.

all of the barrel's length. If, at the time the projectile is halfway down the barrel, the last half of the rail is energized and the previous half is decoupled, the energy represented by the shaded area would not be needed. The energy savings is about 25% for two stages as compared with one.

Figure 15 plots the relative energy loss vs the number of stages. An accelerator comprising 100 equal-length stages would expend only 12% of the energy that would be spent in heating a single-stage accelerator. (The total energy loss in the rails is approximately proportional to $1/\sqrt{N}$, where N is the number of stages.)

The combined effect of energy savings and operation at near maximum current throughout acceleration is seen in Fig. 16 which shows the required energy, E_{rq}, vs velocity for 1-, 10-, and 100-stage accelerators. The required energy is the sum of the kinetic energy, E_p, of the projectile, the stored inductive energy, E_I, of the rails, and the lost energy, E_L. An accelerator using 100 stages requires little more energy than a lossless accelerator. Furthermore, most of the inductive energy remaining in the rails could be recovered. In that case the energy expended would diminish toward the sum of the kinetic energy and lost energy.

Design Criteria. A 10-mm bore will be used for comparison even though a multistage railgun will experience a lower resistive voltage drop than a single stage railgun. Hence this would allow a smaller bore without spurious voltage breakdown.

I discuss two criteria used to divide the MSRG into n sections, one of equal length and the other equal transit time. Table 3 summarizes the operational relationships, where n is the nth stage of an N-stage accelerator.

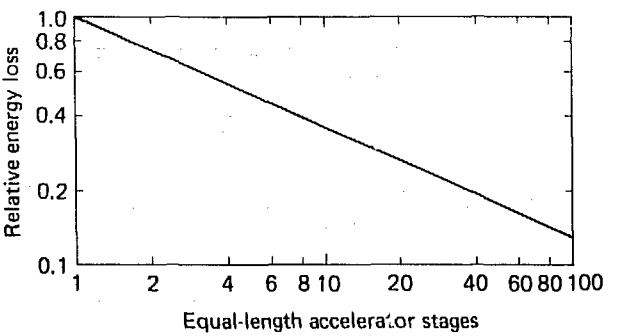

FIG. 15. Relative energy loss vs number of equal-length accelerator stages.

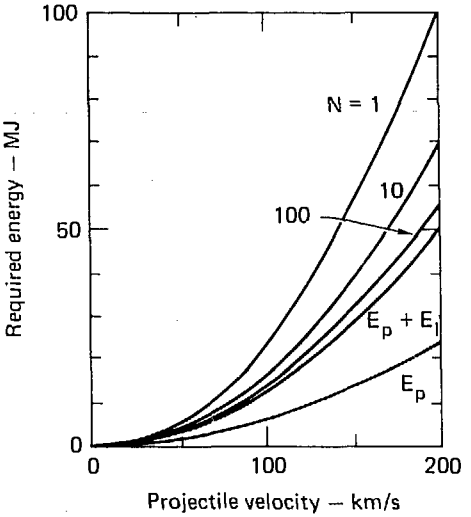

FIG. 16. Required energy for 1-, 10-, and 100-stage railguns. These plots show combined effect of energy savings and operation at near maximum current throughout acceleration. (Table 2 parameters; initial current of each stage = 750 kA.)

TABLE 3. Operational relationships for an N-stage railgun accelerator.

Parameter	Type of multistage railgun	
	Equal length	Equal transit time
Length, G(n)	$\frac{mv_F^2}{L_1 I^2}\left(\frac{1}{N}\right)$	$\frac{mv_F^2}{L_1 I^2}\left(\frac{2n-1}{N^2}\right)$
Transit time, t(n)	$\frac{2mv_F}{L_1 I^2}\left(\frac{n^{1/2}-(n-1)^{1/2}}{N^{1/2}}\right)$	$\frac{2mv_F}{L_1 I^2}\left(\frac{1}{N}\right)$
Kinetic energy increase, $E_p(n)$	$\frac{mv_F^2}{2}\left(\frac{1}{N}\right)$	$\frac{mv_F^2}{2}\left(\frac{2n-1}{N^2}\right)$
Energy loss in rail, $E_L(n)$	$E_N\left[\frac{\left(n^{1/2}-(n-1)^{1/2}\right)^{3/2}\left(2n^{1/2}+3(n-1)\right)^{1/2}}{5N^{5/4}}\right]$	$E_N\left(\frac{n-3/5}{N^{5/2}}\right)$
Exit velocity, v(n)	$v_F\left(\frac{n}{N}\right)^{1/2}$	$v_F\left(\frac{n}{N}\right)$

$$E_N = \frac{16}{3pI}(\pi\mu_0\rho)^{1/2}\left(\frac{m}{L_1}\right)^{3/2} v_F^{5/2}$$

Figure 17 shows the transit time, t(n), energy loss, $E_L(n)$, and energy required $E_{rs}(n)$ in each stage. It also shows exit velocity, v(n), for a 100-stage, equal-length accelerator having the parameters in Table 2 and the initial current of each section equal to 750 kA. The required energy for each module ranges from 670 to 530 kJ.

Likewise, Fig. 18 shows energy required, section length, and velocity for a 100-stage, equal transit-time MSRG accelerator. The required energy of the modules ranges from 5 to 1130 kJ, and the length of each stage ranges from 0.02 to 4.2 m. A design close to the equal-length module appears most practical. A design based on equal required energy for each module would be similar to the equal-length design.

Operational Requirements. The major requirement for successful operation of a multistage railgun is that the energy supplied to each stage be used to accelerate the projectile and not be allowed to propagate back toward the breach. There are several possible methods for fulfilling this requirement.

Pulse Shaping. The input pulse can be shaped to end at the time the projectile leaves each stage. This can be accomplished with saturable reactors[25] or with pulse lines.

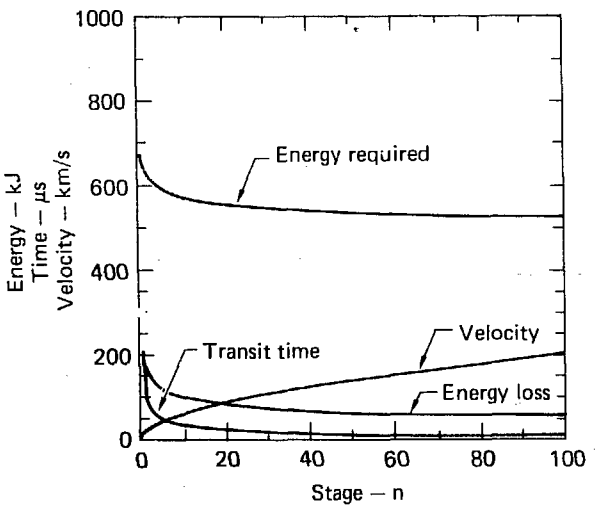

FIG. 17. Energy, transit time, and velocity for 100-stage accelerator with equal-length stages. (Fig. 16 parameters.)

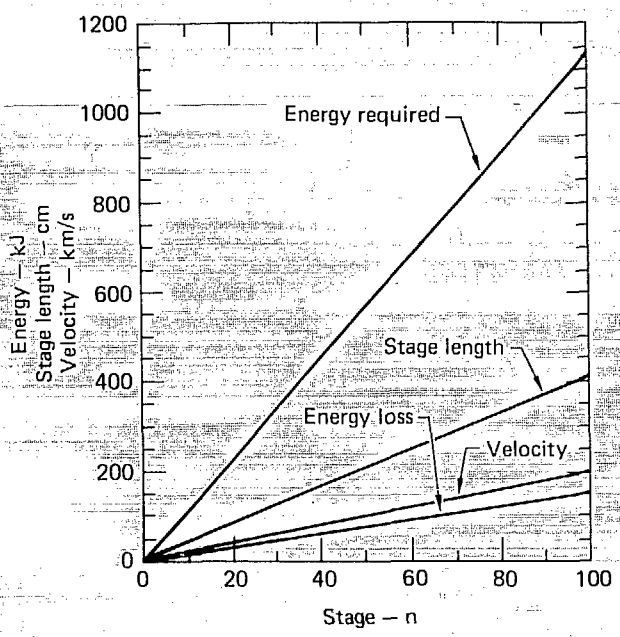

FIG. 18. Energy, stage length, and velocity for 100-stage accelerator with equal transit-time stages. (Fig. 16 parameters.)

Diode Isolation. The current input to each stage could be by way of a diode so current could not flow into a previous stage's energy supply system.

Arc Extinction and Restriking. The arc could be extinguished at the end of each stage and restruck at the beginning of the next. Dielectric isolation of the stages would prevent energy from traveling toward the breach. In this case the arc must be restruck and moved in behind the projectile. Figure 19 illustrates this approach.

As the projectile enters a section, an arc is formed in the side-track rail with the aid of a fuse wire. The side tracks are insulated from the projectile flight path by a dielectric insulator. The arc is accelerated down the side track and timed to arrive behind the projectile as the projectile passes the "Y" junction. Timing is provided by optical, electronic, or other means of sensing the projectile position and velocity.

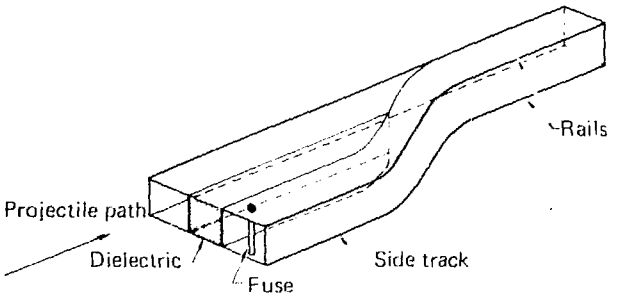

FIG. 19. Side track used to initiate an arc shuttled in behind projectile as projectile passes "y" junction of each stage.

Arc extinction could be provided by

- Activating a shorting crowbar across the end of the stage at the time the projectile leaves the stage. The current could continue to flow and could be used to recharge the source capacitor.
- Using a capacitor as a crowbar to extinguish the arc. The capacitor could store the remaining energy in the inductance of that stage and any energy continuing to be delivered by the source.

Recovered energy could be used on another stage further down the accelerator or be saved for the next projectile.

In summary, multistage accelerators offer more design flexibility and better performance than single-stage accelerators. This results in shorter accelerators, higher efficiency, and less total energy required.

2.3 OTHER CONSIDERATIONS

2.3.1 Use of Sabot Mass

As discussed above, the minimum basic bore size is established by the potential for spurious arc discharge. Minimum bore size combined with a reasonable aspect ratio leads to a minimum sabot volume whose density results in a minimum sabot mass. Because the payload mass (0.1 g) is small compared

with the above arrived-at sabot mass (1.13 g), the conversion efficiency of the initial energy into payload kinetic energy is small.

If the sabot mass could be used for ignition of fusion, the efficiency of a single-stage accelerator would be in the vicinity of 25% instead of 2% (Fig. 13). If, on the other hand, the sabot is not useful, the net efficiency could be improved by increasing payload mass without increasing sabot mass. The value of a larger payload depends on its being useful to DT ignition. For the sake of this discussion, I will assume that is the case.

Figure 20 shows net efficiency, required energy, and expended energy as a function of payload mass for a 100-stage accelerator with an exit velocity of 200 km/s. The advantage of increasing payload mass is clear; this reasoning also applies to the single-stage accelerator.

Table 4 summarizes efficiencies for several combinations of options. The efficiency-of-energy transfer can range from about 2%, for a 0.1-g payload launched with a 1.13-g sabot in a single-section accelerator without any recovery of stored inductive energy, to about 78%, where sabot mass is a useful payload in a 100-stage accelerator with complete inductive energy recovery. Practical and appropriate design depends on the specific way kinetic energy would be used to initiate thermonuclear fusion.

TABLE 4. Efficiencies of converting initial stored energy into payload kinetic energy for single- and 100-stage accelerators. Sabot mass = 1.13 g; launch velocity = 200 km/s.

Accelerator	Without inductive energy recovery (%)	With inductive energy recovery (%)
Single-stage		
0.1-g payload	1.8	2.16
1.0-g payload	9.5	11.3
1.13-g sabot as payload	22	26.6
100-stage		
0.1-g payload	3.5	6
1.0-g payload	19	33
1.13-g sabot as payload	44	78

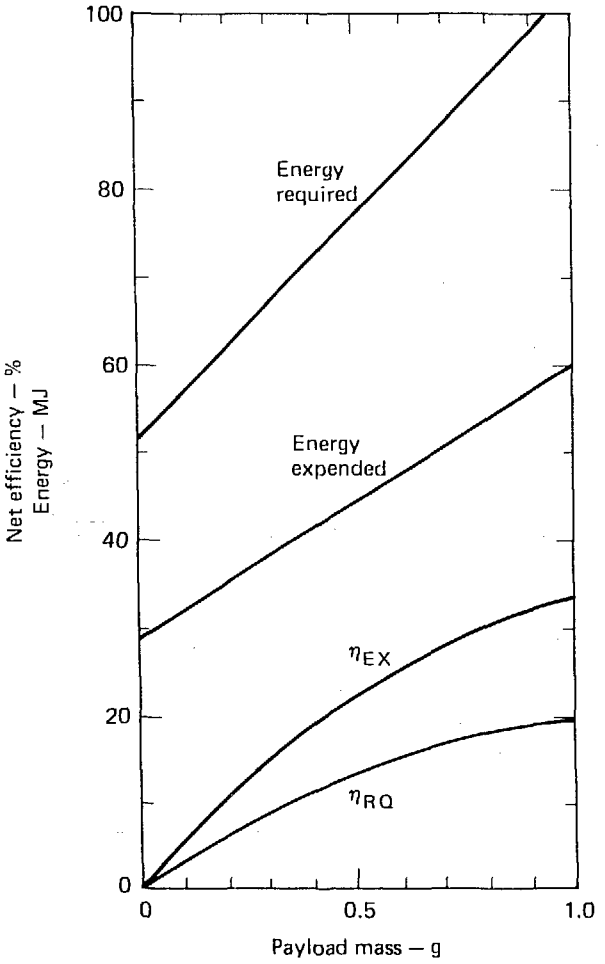

FIG. 20. Net efficiency, required energy, and expended energy for 100-stage accelerator with launch velocity of 200 km/s. (Table 2 parameters except $m_{p\ell}$.)

2.3.2 Cryogenic Rails

Cryogenic cooling of the rails lowers initial resistivity, which leads to less resistive energy loss. It also allows a higher current density to be used without melting the rails (Fig. 6). These advantages would need to be

weighed against the added complexity of the system. Furthermore, rapid repetitive launching would put severe requirements on the cryogenic cooling system.

2.3.3 Heat Transfer From Rails

The rate of heat transfer from the rails will limit the maximum repetition rate of projectile launches. The worst case is at the breach end where about 50 kJ per rail per meter per launch are dissipated. Because the rails must be electrically insulated, they must be cooled by means of conduction through the dielectric insulation or liquid coolant forced through channels in the rails. Using aluminum oxide ceramic dielectric with nominal dimensions, the heat generated in the rails with each pulse could be conducted to the barrel in about 1 s without difficulty. However, most other dielectric materials will not be sufficient thermal conductors for such launch rates. Fluidic cooling is capable of removing the heat at rates up to 1 launch/s. Higher launch rates would require careful design to avoid increased temperatures, resistance, and energy loss.

2.4 SUMMARY

In this part of the report, I described the operating principles of a railgun system, development of a simulation code, practical limitations and their effects on railgun design, and results of calculations. If one uses a large enough primary-energy-storage device or several smaller storage devices, one sees an encouraging possibility: acceleration of a 0.1-g or more payload, mounted in a 1.13-g or less sabot, to 150 km/s or more.

3. COMPARISON OF MAGNETIC-GRADIENT, ELECTROSTATIC, AND RAILGUN ACCELERATORS

This report (Parts 1 and 2) summarized a preliminary study of electrostatic and magnetic accelerators. We wanted to determine if such accelerators might be used to launch a 0.1-g payload to 150 km/s or more. We analyzed first order designs for both magnetic-gradient and railgun accelerators. Our analyses led to the following conclusions.

3.1 MAGNETIC-GRADIENT ACCELERATOR

Regarding the magnetic-gradient accelerator, we concluded that

- A superconducting projectile, with a critical field of 10 T, requires a 3.2-km-long accelerator with a traveling field gradient of $2.5(10^3)$ T/m. This projectile could achieve an efficiency as high as 92%.
- A ferromagnetic projectile requires a 12.4-km-long accelerator and could achieve an efficiency as high as 75%.
- An ablatable copper-sheathed projectile requires a 31-km-long accelerator and could achieve an efficiency as high as 0.3%.
- An unsheathed copper projectile would melt before achieving the velocity goal.

3.2 ELECTROSTATIC ACCELERATOR

Regarding the electrostatic accelerator, we concluded that the required length would need to be greater than 20 km. Thus, this accelerator is not competitive with magnetic accelerators.

3.3 RAILGUN ACCELERATOR

Regarding the railgun accelerator, we concluded that

- A plasma-arc armature is vastly superior to a sliding-metal armature.
- A projectile-launcher system can be designed to avoid adverse effects from boundary layer drag.
- Properties of launcher and projectile materials impose limits on railgun operation.
- Within the operational limits, a railgun appears capable of launching a 1.13-g sabot with a 0.1-g payload at a velocity greater than 150 km/s. The railgun would require the following:
  (1) The launcher must be at least 115 m long.
  (2) A single-stage accelerator would require a primary energy-storage device (of ~60 MJ) and could have an energy conversion efficiency of about 2.0% for the payload and about 25% for the combined mass of the payload and sabot.

(3) A 100-stage accelerator would require a total energy of about 35 MJ and could have an energy conversion efficiency of about 3.6% for the payload and about 44% for the combined mass of payload and sabot.

(4) Further improvements in the design of a multistage accelerator are possible. Hence, this accelerator would be shorter and more efficient.

4. RECOMMENDATIONS

We conclude that traveling magnetic-gradient and railgun accelerators have the potential to launch a 0.1-g payload to hypervelocities (150 km/s or more). To realize this potential, both types of propulsion devices will require further detailed design together with a sequence of critical experiments. These experiments should be designed to determine the limits of operation to minimize accelerator cost and length and to maximize launch velocity and energy conversion efficiency.

We recommend that the first few stages of each accelerator be designed in detail and be experimentally tested. If the results are as encouraging as predicted in this report, more stages could be constructed and again tested. This procedure could be repeated until an insurmountable limit is reached or the goal is attained.

ACKNOWLEDGMENTS

I am pleased to express gratitude to those persons who assisted in my (Part 2) study. Specifically, I appreciate the program support of Don Meeker, John Nuckolls, and Andy Poggio. This study greatly benefited from the support of a separate project sponsored by John Kury to study and initiate a 5- to 40-km/s railgun research program in which Jon Scudder and I participated. Furthermore, I received invaluable technical assistance from Tom Burgess, Jim Brittingham, Alfred Buckingham, Fred Deadrick, Richard More, Steven Moxan, Harry Sahlin, and Jim Shearer.

Finally, I sincerely appreciate the help and patience of Susan Boichat and Larry Gottlieb in preparing the manuscript.

REFERENCES

1. E. R. Harrison, "Alternative Approach to the Problem of Producing Conducting Thermonuclear Power," *Phys. Rev. Lett.* 11, 535 (1963).
2. F. Winterberg, "Attainability of Fusion Temperatures under High Densities by Impact Shock Waves of Microscopic Solid Particles Accelerated to Hypervelocities," *Am. Phys. Soc. Bull.* 9, 308 (1964).
3. F. Winterberg, "On the Attainability of Fusion Temperatures Under High Densities by Impact Shock Waves of Small Solid Particles Accelerated to Hypervelocities," *Z. Naturforsch.* 19a, 231 (1964).
4. C. Maisonnier, "Macroparticle Accelerators and Thermonuclear Fusion," *Nuovo Cimento* 42B, 332 (1966).
5. G. Linhart, "Acceleration of Projectiles to Hypervelocities," in *Proc. Intern. School Enrico Fermi* (Academic Press, New York, 1971), p. 151.
6. F. Winterberg, "Nuclear Fusion by Magnetic Acceleration of a Superconducting Solenoid," *Nucl. Fusion* 6, 152 (1966).
7. F. Winterberg, "Magnetic Acceleration of a Superconducting Solenoid to Hypervelocities," *J. Nucl. Energy* 8, 541 (1966).
8. J. P. Barber, *The Acceleration of Macroparticles and a Hypervelocity Electromagnetic Accelerator*, Ph.D. thesis, Australian National University, Canberra, Australia (1972).
9. R. L. Garwin, R. A. Muller, and B. Richter, *Magnetic-Gun Ignition for Controlled Thermonuclear Fusion*, SRI International, Arlington, Virginia, Tech. Rept. JSN-77-20 (1978).
10. H. H. Kolm, "Basic Coaxial Mass Driver Reference Design," in *Proc. 3rd Princeton/AIAA Conf. Space Mfg. Facilities, 1977.*
11. R. S. Hawke, "Railgun Accelerator for Launching 0.1-g Payloads at Velocities Greater Than 150 km/s," presented at *DOE Impact Fusion Workshop, Los Alamos Scientific Laboratory, Los Alamos, New Mexico, 1979*, proceedings to be published; also, published by Lawrence Livermore Laboratory, Livermore, Calif., UCRL-82762 (1979).
12. D. E. Brast and D. R. Sawle, "Study of Rail-Type MHD Hypervelocity Projectile Accelerator," in *Proc. 7th Symp. Hypervelocity Impact, Tampa, Florida, 1964* (Martin Company, Orlando, Florida, 1965), vol. 1, p. 187.

13. R. L. Chapman, D. E. Harens, and G. P. Sorenson, "The Magnetohydrodynamic Hypervelocity Gun," in *Proc. 6th Symp. Hypervelocity Impact, Cleveland, Ohio, 1963*, vol. 1, pp. 317-330.

14. S. C. Rashleigh and R. A. Marshall, "Electromagnetic Acceleration of Macroparticles to High Velocities," *J. Appl. Phys.* 49, 2540 (1978).

15. R. S. Hawke and J. K. Scudder, "Magnetic Propulsion Railguns: Their Design and Capabilities," presented at *2nd Intern. Conf. Megagauss Magnetic Field Generation and Related Topics, Washington, D. C., 1979*, to be published; also, published by Lawrence Livermore Laboratory, Livermore, Calif., UCRL-82677 (1979).

16. R. A. Marshall, "The 'Flying Fuse' in ANU Rail Gun," in *Proc. 27th Mtg. Aeroballistic Range Assoc. at Commissariat a l'Energie Atomique, Paris, France, 1976.*

17. M. J. Druyvesteyn and F. M. Penning, "The Mechanism of Electrical Discharges in Gases of Low Pressure," *Revs. Mod. Phys.* 12, 87 (1940).

18. R. More, Lawrence Livermore Laboratory, Livermore, Calif., private communication (1979).

19. R. D. Richtmyer and K. W. Morton, *Difference Method for Initial-Value Problems* (Interscience Publishers, New York, 1967).

20. R. E. Kidder, *Nonlinear Diffusion of Strong Magnetic Fields into a Conducting Half-Space*, Lawrence Livermore Laboratory, Livermore, Calif., UCRL-5467 (1959); also H. Knoepfel, *Pulsed High Magnetic Fields* (North Holland Publ. Co., Amsterdam, Netherlands, 1970), p. 80.

21. R. Werne, Lawrence Livermore Laboratory, Livermore, Calif., private communication (1979).

22. W. Nellis, Lawrence Livermore Laboratory, Livermore, Calif., private communication (1978).

23. R. Hackman, "Effects of Voltage Polarity, Electric Current, External Resistance, Number of Sparkings, Supply Frequency, and Addition of Hydrogen and Air on Electrical Breakdown in Vacuum," *J. App. Phys.* 46, 3789 (1975).

24. B. Carder, Lawrence Livermore Laboratory, Livermore, Calif., private communication (1979).

25. K. Aaland, Lawrence Livermore Laboratory, Livermore, Calif., private communication (1979).

APPENDIX A.

THEORETICAL PREDICTION OF EROSIVE DRAG

(Prepared by A. C. Buckingham)

This appendix presents results of theoretical calculations of erosive projectile-rail interactive drag. These results are based on

- Metal-to-metal contact friction exclusively.
- Metal-to-metal contact friction followed by Couette-flow liquid-metal melt layer-boundary layer drag.
- Ablative-material sliding friction followed by Couette flow multicomponent ablation product drag and unconstrained (pregapped) projectile-to-rail clearance Couette flow drag. The initial conditions within the clearance gap assume it is filled with trapped vapor-ablation products at a pressure of 1 atm. These products are assumed developed from previous launches. The assumption is conservative (more erosive than a vacuum gap).

Assumptions and critical features of the theoretical model are summarized in this appendix together with a few references containing more detailed information.

In general, the tightly constrained projectile, particularly the all-metal design, is unsuitable for hypervelocity launch since it will be almost completely consumed by frictional heating and melt. One possible exception would be a projectile banded by ablation material. In this case, even if the projectile is initially tightly constrained, I predict a surface recession gap and intervening ablation erosion-product film layer will develop, separating the solid contact surfaces. This will lower the heating and drag sufficiently so that hypervelocity launch appears possible. Provision of even a modest (1 mil, 2.54×10^{-5} m) gap initially would insure projectile survival under any of the launch circumstances modeled.

My predictions suggest several projectile configurations and materials as promising candidates for hypervelocity launch. These should be tested in successively more severe (higher velocity) railgun launch experiments. Such experiments would verify and substantially enlarge our knowledge of material response, aerodynamic performance, heating, drag, and design considerations for hypervelocity projectiles.

ENERGY BALANCE

A separate publication of the drag/erosion energy dissipation analysis is in final preparation.[1] This appendix will thus be limited to a summary of my findings. A more complete account is in the referenced publication.

The frictional drag, heat, and mass-transfer contributions (together with energy dissipated in melting or ablation of guidance rails or projectile) add up to the drag work done in accelerating a 1-cm × 1-cm × 0.5-cm rectangular parallelepiped-shaped projectile (Fig. A-1). Acceleration is by means of a magnetically driven plasma field at the projectile base.[2] The projectile "payload" is completely enveloped by a sabot, which consists of homogeneous material and which has a fixed overall shape and dimensions as given.

For the metal (steel) projectile/sabot material estimates, I use the thermodynamic, transport, and material properties of iron. This initial metallic projectile/sabot mass is 3.75×10^{-3} kg. For the carbon (graphite) and Teflon sabot surrounding a metallic projectile, I use the appropriate (graphite or Teflon) properties. However, the accelerated initial mass for either material is the same, 1.2×10^{-3} kg. From the estimates given in the main body of this report as well as in Hawke and Scudder,[2] I can compute the accelerating force in the railgun as

$$F = L_1 I^2/2 \ , \tag{A-1}$$

where

$$L_1 = \frac{\text{inductance}}{\text{unit length}} = 4.2 \times 10^{-7} \text{ H/m} \tag{A-2}$$

and

$$I = \text{current density} = 0.75 \text{ MA/cm} \ . \tag{A-3}$$

Hence $\vec{F} = 1.81 \times 10^{-5}$ N, the estimated maximum propulsion force.

The acceleration, considered constant throughout launch, can then be computed for the metal sabot/projectile:

$$a = 3.1 \times 10^{7} \text{ m/s}^2 \ ; \tag{A-4}$$

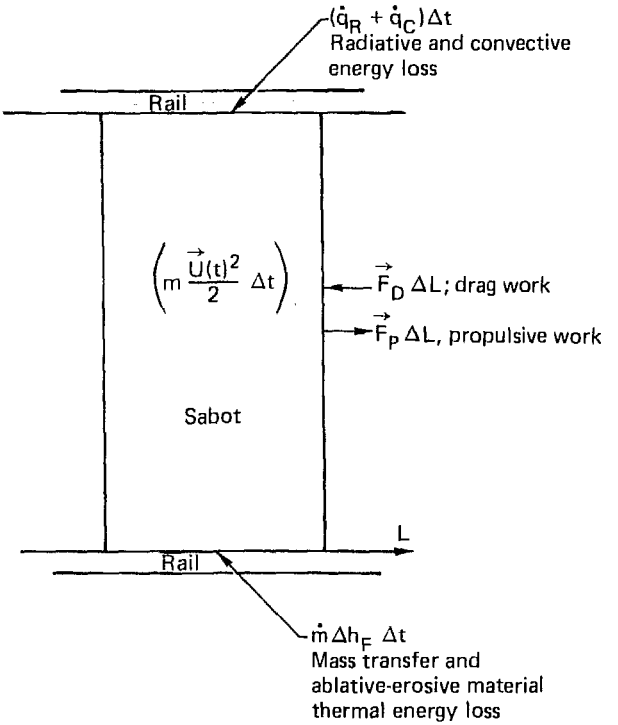

FIG. A-1. Energy balance for projectile-sabot configuration. ($w = h = 2\ell = 10$ mm.)

while that for the graphite sabot/projectile is

$$a = 9.8 \times 10^7 \text{ m/s}^2 . \qquad \text{(A-5)}$$

The energy balance on the projectile/sabot system during launch is shown schematically in Fig. A-1. For my calculations, I consider contributions from the frictional drag, projectile/rail heat transfer, mass transfer, phase change, and ablation/erosion as the total drag "debt" paid by the available propulsion energy. The resulting energy balance equation is expressed in integral work (moment of momentum) form by first multiplying Newton's law of motion by the differential work path, $d\vec{s} = \vec{U}dt$, then performing the

integration. This integral form is convenient for programming:

$$\int_{t=0}^{t'} \vec{F}_p \, \vec{U}(t) \, dt - \frac{1}{t'} \int_{t=0}^{t'} \frac{m(t) \, \vec{U}(t)^2}{2} \, dt - \int_{t=0}^{t'} A(t) \left\{ \dot{q}_R + \dot{q}_C \right\} dt$$

$$-\Delta h_F \int_{t=0}^{t'} \dot{m}_F \, dt - \int_{L(t=0)}^{L(t=t')} \sigma_W \, ds = 0 \, . \qquad \text{(A-6)}$$

The first term in Eq. (A-6) represents the propulsive work accumulated from initiation of motion (t = 0) until some time, t', and acceleration of the projectile to a velocity, $\vec{U}(t)$, with propulsive force, $\vec{F}_p = m(t)a$. The mass of the projectile, m(t), is continually being reduced by erosive-material loss due to friction and heating.

The second term expresses the work associated with the change in kinetic energy of the projectile over the time interval, $\Delta t = t'$.

The third term is the work invested in combined radiative, $\dot{q}_R$, and convective heating, $\dot{q}_C$, to both the contact rails and sabot over the effective surface area, A, influenced by the heat transfer.

Heat energy loss due to melting and vaporization, Δh_F, over the rate of change of material mass, $\dot{m}_F$, undergoing irreversible phase change within this time interval, is given by the fourth term.

The fifth and last term of the energy balance expresses the shear-frictional loss. This appears as the integrated product of the various components of wall friction force (σ_W from liquid, solid, vapor boundary layer, and sliding friction) with the distance s = L(t') - L(0) over which the force acts.

Equation (A-6) is programmed for time-incremental, Δt, integration at automatically selected steps. The nonlinear contributions of velocity change; mass change; and effects on heat, mass, momentum, and thermo-chemical state changes are combined through use of an implicit (iterative) algorithm applied at each time step. I imposed time-step control using a periodic Jacobian evaluation for derivative magnitudes. This was necessary because of the inherent "stiffness" of Eq. (A-6), which develops from the imbalance in relaxation times between accelerations, $d\vec{U}/dt$, and mass changes, dm/dt.[1]

METAL-TO-METAL FRICTION,
SUBSEQUENT LIQUID-METAL BOUNDARY LAYER

The metal-to-metal, rail-sabot contact friction was computed from an upper limit estimate[2] normal force $F_\perp$, and a variable coefficient of sliding friction, C_F. This coefficient, obtained from low speed sliding data,[3] is not applicable at hypervelocity where material degeneration (particulate separation and thermal ablation) is expected. This expectation is based on established material degradation observed in an arc jet and shock tube material erosion test at equivalent energy levels.[4,5] To model this, I supplemented the sliding friction force, initially computed from

$$\sigma_W = C_F F_\perp \quad , \tag{A-7}$$

by either liquid-metal film or ablation-erosion (two-phase) film layer calculations where appropriate. The normal force in the initial calculations is considered a maximum value associated with a material stressed beyond its yield limit by the applied propulsive force.[2] The acceleration force equals the normal force for this "strengthless" limit.

The supplemental-film layer or liquid-metal layer film calculations are outlined in the next section. They are modeled with boundary layer approximations applied to the Couette flow of the film in the contact region. The limited amount of data available are extrapolated from reentry heat shield material degradation experiments[4,5] and metallic impact or explosive welding experiments. Material ablation/erosion/corrosion response data used for the present estimates include supplemental correlations developed from analysis of these and similar experiments.[6,7] Lack of experimental verification of hypervelocity contact-material degeneration, heat transfer, friction, and resulting drag is a major consideration for basic information and verification sought in our subsequent railgun launcher experiments.

Representative levels of C_F for the "film" coefficients deduced from the above sources are 0.02 and 0.04 for the graphite and Teflon sabots. I postulate that the reduction in contact drag for a deteriorating material contact interface primarily results because of film separation (lubrication) and solid particulate impregnation of the natural roughness "valleys." This leaves an effectively smoother hydraulic sliding surface.

The liquid-metal melt layer film subsequently forms despite the high impact (or normal stress) in impact welding primarily because of the dynamic situation. Here the melt layer is conceptually removed as fast as it forms. This is caused by boundary layer convection, initiated and driven by a wave motion impulse spreading from the solid region to the liquid-metal penetration layer. The penetration layer is small (1 μm) because of the lack of time for thermal diffusion to spread the melt through the metal during impact or during explosive-welding energy deposition. I applied a similar assumption to my estimates since the entire launch phase is only of the order of 1 to a few ms for any of the launch situations modeled.

Figure A-2 gives the drag-free trajectory (distance vs time) and velocity vs time launch history. It also shows the propulsive energy for a constant-mass graphite sabot projectile combination, configured as in Fig. A-1. The mass in this example calculation is 3.75×10^{-3} kg; it is constant in the drag-free limit.

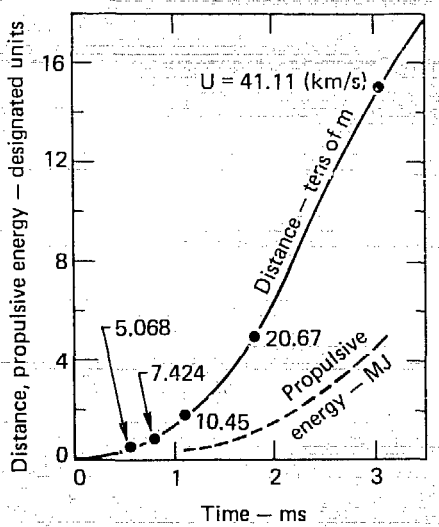

FIG. A-2. Drag-free trajectory, speed, and propulsive energy expended for 3.75-g (steel) projectile.

A seeming paradox develops in reviewing predicted results on some of the materials in which significant drag, heating, and resulting erosion occur. They travel farther in less time. This, however, is the result of applying a constant accelerating force to a projectile whose mass is rapidly diminishing. Because of the corresponding gap that develops between eroding projectile and rails during launch, some configurations, particularly the metallic contact sabot, conceptually fail well before they are consumed by erosive friction and heating. The gap between projectile and rail grows until it cannot seal off excessive plasma leakage about the projectile.

If one considers sliding friction (and film-contact melt friction) alone (without allowing for the complete liquid-metal boundary layer to form), this results in the situation depicted in Fig. A-3, where only a fractional distance of rail launcher is traveled before the drag energy to propulsive energy, E/E_p, and projectile mass to initial mass, m/m_0, indicate that the metallic projectile fails. A more reasonable model, based on the boundary layer-Couette flow momentum integral constraint described in the next section, is shown in Fig. A-4. In this case the gap conceptually "grows" sufficiently so that the sum of the normal momentum due to mass transfer from the melting surface and the momentum integral taken over the boundary layer gap balance

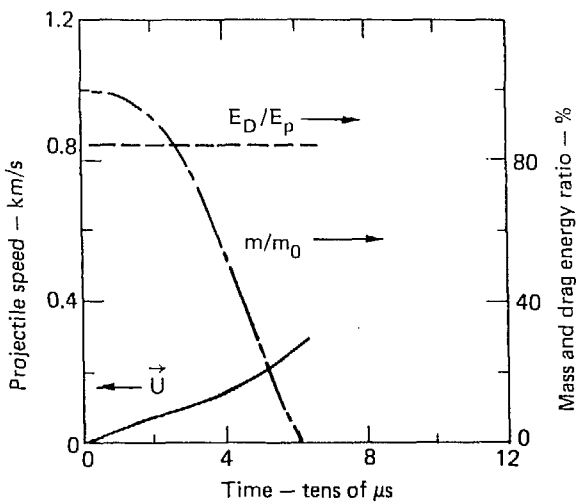

FIG. A-3. Projectile launch history for metal-to-metal sliding friction with instantaneous melt (exclusively).

and equilibrate the normal force, $F_\perp$. At this time and later in the particular launch event, the drag, heat transfer, and erosion results are computed using the Couette flow-boundary layer model for liquid-metal (steel). The results shown in Fig. A-4 are still not favorable for steel sabots. However, the use of other, high temperature metals, particularly refractory metals, perhaps in combination with sacrificial ablative bands surrounding them, remains promising. They are definite candidates for railgun launch experiments.

EROSIVE MULTIPHASE/COMPONENT BOUNDARY LAYER RESULTS

Subsequent to film layer formation, I used Couette flow calculations to model the erosive heat transfer and drag either for the final liquid metal layer predictions (Fig. A-4) or for the erosive graphite and Teflon calculations discussed here. The switch from film layer to Couette flow is made based on simple momentum-integral normal force constraint introduced in the previous section. The boundary layer-Couette flow model includes variable mass density, state, equilibrium and chemically frozen transport properties,

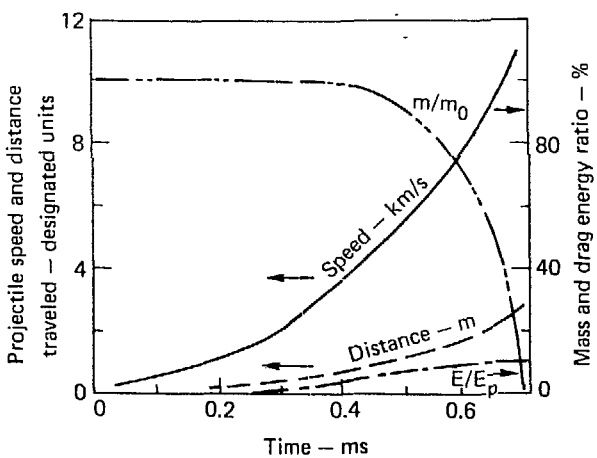

FIG. A-4. Projectile launch history for metal-to-metal sliding followed by liquid-melt erosive drag and heating.

molecular rosive components, and solid phase (carbon) constituents of the eroding surfaces, together with turbulence.

I use the basic integral boundary layer solution technique for reacting multicomponent, multiphase flows developed by Kendall and Bartlett[8] since it models most of the active physical processes one anticipates in erosive heat transfer. Turbulence modeling and nonequilibrium (finite-rate) reactive gas phase and gas-solid chemistry models have been subsequently added by Tong et al.[7,9] while Nicolet et al.[6] reconfigured the technique so quasi-unsteady flow situations could be approximated.

I follow this spirit in generating a quasi-transient solution from a sequence of steady-state solutions by

- Adjusting edge conditions.
- Transforming potential flow conditions at the edge (subscript e) of the predicted steady-state flow field.
- Transforming to include transient rate-of-growth of the boundary layer.

Potential flow edge conditions are transformed by the Euler streamwise approximation

$$\frac{\partial \tilde{U}_e}{\partial t} \sim \tilde{U}_e \frac{\partial \tilde{U}_e}{\partial x} \quad . \tag{A-8}$$

Rate-of-growth is achieved by transforming the normal to-the-surface, y, spatial coordinate within the boundary layer

$$\bar{\eta} = \int_0^{y^*} \frac{\rho(y)}{\rho_e} \, dy/2\sqrt{\nu t} \tag{A-9}$$

In Eqs. (A-8) and (A-9), $\tilde{U}_e$ is the mean "edge" potential velocity replaced in my Couette flow analogy by the instantaneous projectile speed, t is physical time, $\rho(y)$ is the density profile computed in the boundary layer solutions, and ρ_e is the "edge" density. The physical coordinate, y, is taken to be zero at the stationary rail and $y_e = \delta$ is the gap thickness at the moving projectile. The "kinematic" viscosity, ν, is the ratio of the local viscosity coefficient to the mass density.

The transformation, Eq. (A-9), incorporates compressibility effects through the density ratio stretching (good) but is rigorously self-similar

only for *nonreactive laminar* boundary layers with constant viscosity (bad). At present, we at Lawrence Livermore Laboratory are developing solutions for the generalized three-dimensional (unsteady) reacting boundary layer for erosive flow predictions.[10] However, these will not be ready for application until a later (analysis) stage of the railgun experiments.

My present calculations are very general and numerically exact approximations to erosion, drag, and heating with the exception of the assumptions on quasi-unsteady flow given in the previous paragraph. I applied mass, momentum, and energy constraints to the wall surface. This surface is modeled, quite generally, with solid particulate (blowing) fluence; gas phase and gas-solid surface reactions; energy; and mass transfer. For other details of the formulation and modeling of other erosive flow situations[10] as well as the present one,[1] I invite the reader's attention to the cited references.

I want to introduce one other consideration, that of laminar vs turbulent flow, before proceeding with a discussion of current results. My calculations are primarily made for fully developed turbulent flow, although a few of the results (much less erosion, drag, and heating) for laminar flow are shown for comparison. This is an *overly* conservative estimate.

The boundary layers will probably be laminar or at most incipient (developing) turbulent boundary layers in our railgun acceleration situations. Two reasons exist for this. Turbulent instabilities may form but not spread (fully develop) in the boundary layer region during the time it takes the projectile to clear the rails, $\mathcal{O}$, (1 ms). This is indicated by an approximate, linear stability analysis on the boundary layer equations. Second, under accelerations such as encountered in railgun launch, evidence exists that even fully developed turbulent boundary layers will regress to their laminar state.[11-14]

The correlations functions obtained from our numerical solutions are

$$\text{graphite} \begin{cases} (Nu)_T = 3.2(10^{-2})Re^{0.8} , & \text{(A-10)} \\ (Nu)_L = 0.686\ Re^{0.5} , & \text{(A-11)} \end{cases}$$

$$\text{Teflon} \begin{cases} (Nu)_T = 4.3(10^{-2})Re^{0.8} , & \text{(A-12)} \\ (Nu)_L = 0.308\ Re^{0.5} . & \text{(A-13)} \end{cases}$$

The subscripts "T" and "L" refer to turbulent and laminar boundary layer results. Re is the Reynolds number of the erosion product layer based on the rail separation distance.

The shear friction force at the wall, τ_w, (in MPa) correlates to the heat transfer as anticipated by Reynolds analogy. I obtain

Teflon

$$\left(\frac{\tau_w}{\dot{q}}\right)_T = 6.76 \times 10^{-7} , \tag{A-14}$$

$$\left(\frac{\tau_w}{\dot{q}}\right)_L = 8.77 \times 10^{-7} , \tag{A-15}$$

graphite

$$\left(\frac{\tau_w}{\dot{q}}\right)_T = 1.07 \times 10^{-7} , \tag{A-16}$$

$$\left(\frac{\tau_w}{\dot{q}}\right)_L = 3.69 \times 10^{-7} . \tag{A-17}$$

Knowing the heat transfer and wall shear as functions of the erosive surface mass, momentum, and energy balances, one may determine the projectile wall recession rates (erosion). The results are functionally approximated in our (narrow) range of interest for material degradation by

$$\text{(carbon)}\ \dot{\Delta y}_w\ (ms^{-1}) = 2.71 \times 10^{-3} (\dot{q})^{1.70} , \quad \bar{Y}^2 = 0.18 \tag{A-18}$$

and

$$\text{(Teflon)}\ \dot{\Delta y}_w\ (ms^{-1}) = 3.48 \times 10^{-3} (\dot{q})^{1.84} , \quad \bar{Y}^2 = 0.12 . \tag{A-19}$$

In Eqs. (A-18) and (A-19), the heat flux $\dot{q}$ in the correlation is in units of (GWm^{-2}). $\bar{Y}^2$ is the variance taken over all the numerical results in the sampling (more than 100 data points from the boundary layer-Couette flow solutions).

The results of these calculations indicate some improvement in the performance of either graphite or plastic sabots over that of pure steel.

Although, in either case, failure of the concept may be realized from excessive leakage of the plasma (too large a gap) as opposed to mass loss, which is relatively minor. Certainly for the launcher experiments, even without an initial (gap) clearance, the graphite or Teflon sabots are much more promising than is the pure metal (steel) from the erosion-drag viewpoint.

The results, for assumed turbulent boundary layer (conservative) estimates, are summarized in Fig. A-5 for the graphite projectile and in Fig. A-6 for the Teflon projectile initially confined (no gap) by the normal force equivalent to the acceleration force. I show ratios of mass, m/m_0, and energy, E/E_p, or drag work for either Teflon or graphite that are much more favorable than the pure steel sabot results previously presented. Also depicted is the trajectory (distance vs time; velocity vs time) for the two projectile materials. The Teflon and graphite sabot projectile combinations were assumed to have the same initial mass, $m_0 = 1.2 \times 10^{-3}$ kg.

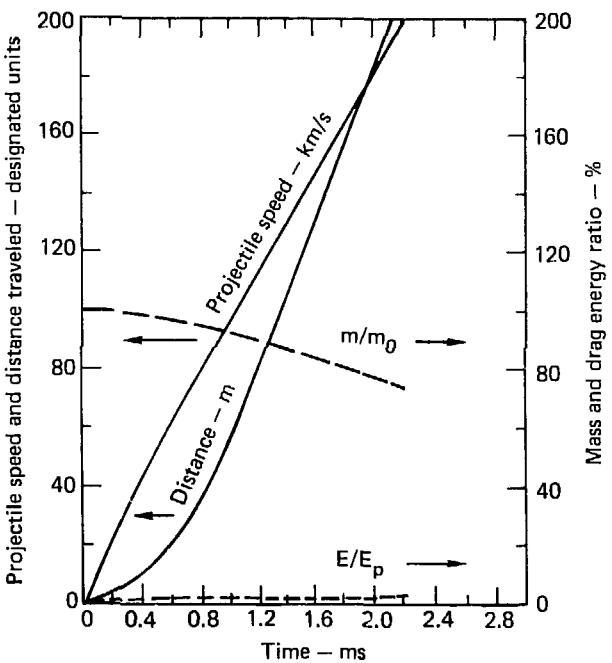

FIG. A-5. Trajectory, energy loss, and mass loss for graphite sabot sliding contact. This is followed by erosive film layer with turbulent Couette loss.

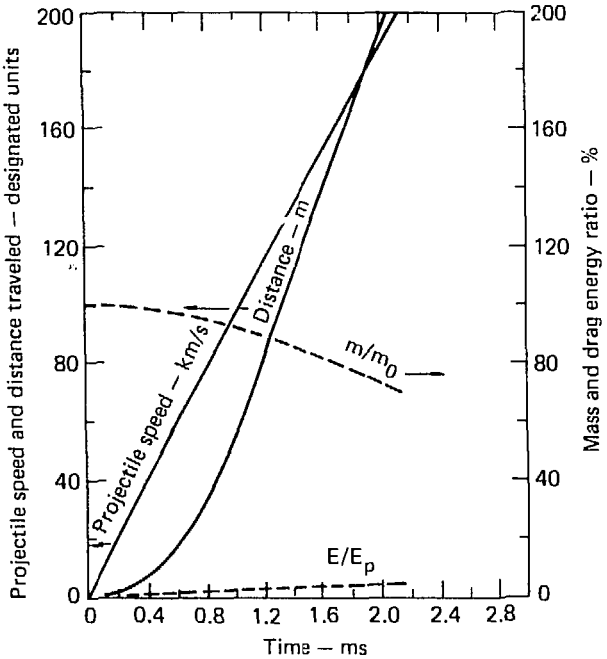

FIG. A-6. Trajectory, energy loss, and mass loss for Teflon ablative-sabot for sliding contact followed by erosive film layer with turbulent Couette loss.

EROSIVE BANDED ABLATORS WITH PRESCRIBED CLEARANCE BETWEEN PROJECTILE AND RAIL

I also investigated the effects (quite significant) of a modest amount of initial gap provided between sabot and rails. Conceptually, no sliding friction is encountered. So only erosive boundary-layer-drag heat transfer and mass transfer are associated with the drag energy expenditure during launch. I assume (for conservatism) that the initial sabot-rail clearance is filled from the start with 1 atm of ablation products. Then I calculate the rate of increased sabot erosion product mass lost and rate of drag following acceleration from this initial state.

Figures A-7 and A-8 are plots of the laminar and turbulent total drag

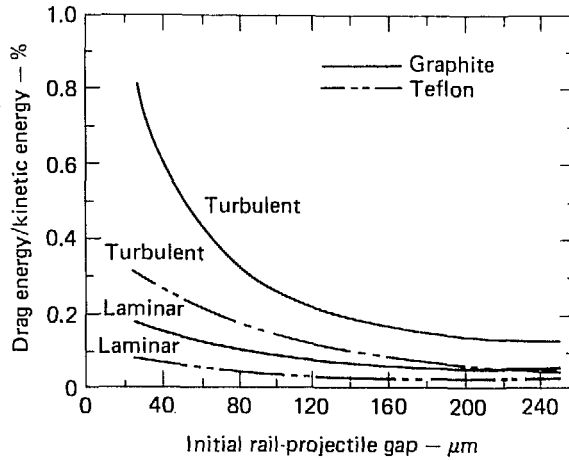

FIG. A-7. Total drag energy expended as percentage of propulsive energy for 200-m rail launcher.

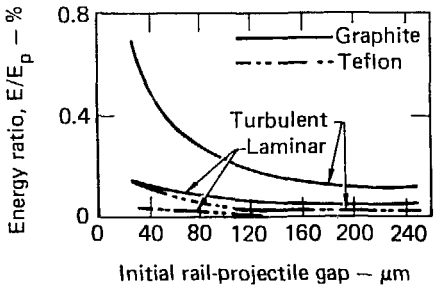

FIG. A-8. Total drag energy expended as percentage of propulsive energy for 100-m rail launcher.

energy in ratio to the propulsive energy for graphite and Teflon sabots at the 200 and 100 m launch positions, respectively.

These results are the most promising of all. Even a modest (1 mil, 2.54×10^{-5} m) initial clearance should be adequate to prevent excessive drag. An additional concern develops, however, in case a clearance gap is used. This concern is directed to the possible occurrence of oscillation and impact between sabot and rails during launch. Ablative bands, which seal the gap and provide ablative product separation layers during launch, may be the answer. These and other conceptual configurations will be examined during the succession of experimental railgun launcher tests.

We anticipate establishing not only successful projectile designs but also verification and extension of critical material response information available for design of hypervelocity projectile launch systems.

REFERENCES

1. A. C. Buckingham, "Rail Guided Hypervelocity Projectile Erosive Drag Predictions," Lawrence Livermore Laboratory, Livermore, Calif., UCRL-82856 in preparation (1979) for presentation at *AIAA 18th Aerospace Sciences Mtg., Pasadena, Calif., 1980.*
2. R. S. Hawke and J. K. Scudder, "Magnetic Propulsion Railguns: Their Design and Capabilities, "Lawrence Livermore Laboratory, Livermore, Calif., UCRL-82677 (1979); presented at *2nd Intern. Conf. Megagauss Magnetic Field Generation and Related Topics, Washington, D. C., 1979.*
3. *American Institute of Physics Handbook*, D. E. Gray, Ed. (McGraw-Hill Book Co., New York, 1957), pp. 2-40, 2-43.
4. M. J. Abbett, F. C. Weiler, and C. A. Powers, *Optimization of Graphite Nosetip Model Thermostructural Tests in the AFFDL 50 MW RENT Facility*, Aerotherm Acurex Corp., Mountain View, Calif., Rept. 72-49 (1972).
5. R. A. Rindal, "High Pressure Ablation Characteristics of Graphite for Nose Tip Applications," in *Graphite Materials for Advanced Reentry Vehicles, Part I*, D. M. Forney Ed., Air Force Materials Lab, Wright-Patterson AFB, Ohio, AFML TR-70-133 (1970).
6. W. E. Nicolet, H. L. Morse, and R. M. Kendall, *Development of Procedures and Selected Predictions for Explosively Driven Flow Fields in Ducts*, Aerotherm Acurex Corp., Mountain View, Calif., Rept. 71-39 (1971).
7. H. Tong, A. C. Buckingham, and D. M. Curry, "Computational Procedure for Evaluation of Space Shuttle TPS Requirements," AIAA Paper No. 74-518, in *Proc. AIAA 7th Fluid and Plasma Dynamics Conf., Palo Alto, Calif., 1974.*
8. R. M. Kendall and E. P. Bartlett, "Nonsimilar Solution of the Multicomponent Laminar Boundary Layer by an Integral Matrix Method," *AIAA Journ.* 6, 1089 (1968).
9. H. Tong, A. C. Buckingham, and H. Morse, *Non-Equilibrium Chemistry Boundary Layer Integral Matrix Procedure*, Aerotherm Acurex Corp., Mountain View, Calif., Rept. 73-67 (1973).
10. A. C. Buckingham, "Propellant Driven Turbulent Interior Ballistics and Wall Erosion," Lawrence Livermore Laboratory, Livermore, Calif., UCRL-81289 (1978); presented at *AIAA 17th Aerospace Sciences Mtg., New Orleans, Louisiana, 1979.*

11. B. E. Launder, "Laminarization of the Turbulent Boundary Layer in Severe Acceleration," *J. Appl. Mech.* 31, 707 (1964).

12. P. M. Moretti and W. M. Kays, *Heat Transfer through an Incompressible Turbulent Boundary Layer with Varying Free Stream Velocity and Varying Surface Temperature*, Stanford Univ., Thermo Sci. Div., Palo Alto, Calif., Rept. PG-1 (1965).

13. F. A. Schraub and S. J. Kline, *A Study of the Structure of the Turbulent Boundary Layer With and Without Longitudinal Pressure Gradients*, Stanford Univ., Thermo Sci. Div., Palo Alto, Calif., Rept. MD-12 (1965).

14. V. C. Patel and M. R. Head, *Reversion of Turbulent to Laminar Flow*, Aero Res. Council, Great Britain, Rept. 29 859 F. M. 3929 (1968).

APPENDIX B.

OTHER METHODS OF ACCELERATING MACROPARTICLES TO 150 km/s

In addition to the three methods discussed in this report (Parts 1 and 2), we considered rockets, gas and explosive guns, and laser ablation techniques.

ROCKETS

In multistage rockets the velocity increase, Δv, of each stage adds to the velocity of the previous stage. The ratio, ν, of payload mass, $m_{p\ell}$ of each stage to the initial mass of the corresponding stage is typically 0.1. The initial mass, m_0, of the whole rocket is

$$m_0 \sim m_{p\ell}\left[\frac{1}{(\nu)^{v_F/\Delta v}}\right] , \tag{B-1}$$

where v_F is the final velocity. If Δv = 10 km/s, a 15-stage rocket would be required to achieve 150 km/s. Furthermore, an initial mass (mostly propellent) of $\sim 10^{11}$ kg would be required.

GAS, EXPLOSIVE, AND EXPLODING-FOIL GUNS

Gas, explosive, and exploding-foil guns can accelerate projectiles up to the expansion velocity of the propellent. Compressed hydrogen, with its low density, is used in the fastest gas guns. The propulsive gas can be pressurized by the first stage of a two-stage gas gun or by explosives. Twenty years of gas and explosive gun development have not substantially increased the launch velocity of a projectile beyond about 10 km/s. Furthermore, there is no hope of going much beyond 10 km/s (Ref. 1).

The exploding-foil technique has recently met with successful launching of milligram dielectric plates at ~20 km/s.[2] Some improvement[3] of this device was obtained by adding rails to the launcher to extend the distance the foil arc could be maintained behind the dielectric, which is similar to

a railgun situation. This technique has promise for an inexpensive high pressure research device. However, its ability to accomplish the goal of this study appears doubtful at this time.

LASER ABLATION

It has been proposed to use a laser to ablate material off the backside of a projectile to reactively accelerate it to hypervelocities[4]. The calculated efficiency of conversion of light energy into projectile kinetic energy was a substantial 10%. If a high efficiency laser (~10%) could be used to ablate the material, an overall efficiency of ~1% might be possible. This technique awaits experimental verification.

REFERENCES

1. W. Nellis and R. N. Keeler, Lawrence Livermore Laboratory, Livermore, Calif., private communications (1979).
2. R. C. Weingart, H. H. Chau, D. R. Goosman, W. W. Hofer, C. A. Honodel, R. S. Lee, D. J. Steinberg, and J. R. Stroud, *The Electric-Gun: A New Tool for Ultrahigh Pressure Research*, Lawrence Livermore Laboratory, Livermore, Calif., UCRL-52752 (1979).
3. R. C. Weingart, Lawrence Livermore Laboratory, Livermore, Calif., private communication (1979).
4. T. E. McCann and J. S. DeGroot, *Acceleration of Solid Macro-Particles by Laser Ablation*, Lawrence Livermore Laboratory, Livermore, Calif., UCRL-79732 (1977).

LG/skg

U.S. Government Printing Office: 1979/11 — 689-102/8739